Comprehensive Analysis of M^{6}A-Related lncRNAs, Immune Checkpoints and Immune Infiltrates in Clear Cell Renal Cell Carcinoma

Lin Hui
Shanxi Medical University Second Affiliated Hospital: Second Hospital of Shanxi Medical University
Zhang Junhua
Shanxi Medical University Second Affiliated Hospital: Second Hospital of Shanxi Medical University
Guo Xiaoyu
First Affiliated Hospital of Harbin Medical University
Wang Lihua
Shanxi Medical University Second Affiliated Hospital: Second Hospital of Shanxi Medical University
Xi Qiao (qiaoxi7347@vip.163.com)
Shanxi Medical University Second Affiliated Hospital: Second Hospital of Shanxi Medical University

Research Article

Keywords: Clear cell renal cell carcinoma, tumor immune environment, m6A-related lncRNAs

Posted Date: February 23rd, 2022

DOI: https://doi.org/10.21203/rs.3.rs-1052999/v1

Abstract

Background

Clear cell renal cell carcinoma (ccRCC) is the most common renal cancer in the world and is strongly related to the tumor immune microenvironment (TIME), which is mediated by N^6 Methyladenosine-related long noncoding RNAs (m^6A-related lncRNAs). In order to explore the underlying effective treatment and prognostic biomarkers, the correlation of m^6A-related lncRNA, TIME with survival deserves in-depth study.

Methods

All the data which include 53 tumor samples as well as 72 normal samples were obtained from The Cancer Genome Atlas (TCGA). Herein, we systematically explored the correlations of prominent m^6A-related lncRNAs with 5 immune checkpoints (CTLA4, TIGIT, PDCD1, CD19 and LAG3) and immune infiltrates. Patients were divided into 2 clusters based on 30 prognostic m^6A-related lncRNAs. Six m^6A-related lncRNA-associated signatures were used to construct a risk model for ccRCC. Following that, we investigated the correlation between m^6A-related lncRNA-associated signatures and immune cells, immune score, and immune checkpoints.

Results

The expressions of these 5 immune checkpoints (CTLA4, TIGIT, PDCD1, CD19 and LAG3) were positively correlated with the expressions of the 30 m^6A-related lncRNAs. Compared to cluster 1, cluster 2 had a higher immunoscore, remarkable immune cell infiltration, upregulated checkpoints and poor prognosis. The hallmarks protein secret, androgen response, adipogenesis, bile acid metabolism, fatty acid metabolism and PPAR signaling pathway were remarkably enriched in the cluster 1. With high-risk scores, patients had higher immunoscore and higher expression of the 5 immune checkpoints. The amount of tumor-infiltrating immune cells was dynamically altered by copy-number changes in m^6A-related lncRNA-associated signatures.

Conclusions

Our research revealed the crucial involvement of m^6A-related lncRNAs in the TIME of ccRCC. The suggested m^6A-related lncRNA-associated signatures might be important mediators of TIME in ccRCC, providing ideal therapeutic targets in immunotherapeutic effectiveness.

Background

Renal cell carcinoma (RCC) is the third most common urinary system cancer globally, with clear cell renal cell carcinoma (ccRCC) accounting for 80% of cases [1]. Chemotherapy is ineffective against ccRCC because of its high angiogenesis and hypoxic tumor environment [2]. For decades, surgical resection has been the best option or most effective treatment. However, even after surgical resection, 20% of patients experience local recurrence or separate metastasis. Therefore, finding more efficient ways of prognosis and treatment is both important and challenging. In this research, we decided to investigate some novel insights on one kind of epigenetic modification, N^6 Methyladenosine (m^6A) of long noncoding RNAs (lncRNAs), as prognostic markers that influence tumor immune microenvironment (TIME) of ccRCC.

LncRNAs have received a lot of attention as epigenetic marks that play essential roles in cancers. Increasingly, lncRNAs are being investigated as potential prognostic indicators or therapy targets in malignancies [3–4]. Abnormal expressions of lncRNAs would lead to different severity of cancers via changing cancer cell proliferation, differentiation, apoptosis, or metastasis. So far, m^6A modification, which refers to adenosine N^6 methylation as the most common, prolific, and conservative internal dynamic post-transcriptional chemical change of numerous non-coding RNAs, has been found in an increasing number of lncRNAs, also known as m^6A-related lncRNAs [5–7]. Under the control of methyltransferases, such as the complex of methyltransferase ("writer"), binding protein ("reader"), and demethylase ("eraser"), m^6A modification can be variable and reversible. METTL3, METTL14, METTL16, RBM15, RBM15B, VIRMA, ZC3H13 are classified as “writers”. YTHD1/2, YTHDF2/3, HNRNPC, HNRNPA2B1, IGF2BP1/2, RBMS, FMR1, LRPPRC are classified as “reader”. ALKBH5 and FTO are classified as “erasers” [7].

Although multiple lncRNAs have been reported to regulate TIME in various tumors, few researches on ccRCC have been done [5–9]. In ccRCC, methylation of lncRNA DMDRMR which is mediated by m^6A reader IGF2BP3 can finally drive tumor prognosis [5]. m^6A modification of lncRNA NEAT1-1 promote the complex cyclinl1/CDK19/NEAT1-1, which is a stimulating factor of bone metastasis in prostate cancer [8]. In colorectal cancer, lncRNA LINRIS stabilizes IGF2BP2 [9]. In order to unearth more m^6A-related lncRNAs that regulate TIME in ccRCC, we decided to use bioinformatics analysis to predict the potential m^6A-related lncRNAs as targets for early diagnosis and therapy.

Immunotherapy based on immune checkpoint antibody is one of the most promising treatment for ccRCC, especially in advanced stage [10]. Anti-CTLA4 immunotherapies, such as ipilimumab and bevacizumab, have shown good results in the treatment of advanced ccRCC [11–13]. Immune evasion and tumor growth are caused by a lack of effective anti-tumor immune responses. Immune checkpoints secreted by immune cells can inhibit the function of immune cells. Some immune checkpoints, including as CTLA4, TIGIT, CD19, PDCD1, and LAG3, have been found in ccRCC [14–17], although their correlations with m^6A-related lncRNAs have yet to be determined [18, 19].

Herein, the goal of this research is to see if there is link between m^6A-related lncRNAs, disease prognosis, immune checkpoints and TIME in ccRCC. To enhance the prognosis risk classification and therapeutic

decision-making of ccRCC patients, a risk model that focuses on m^{6}A-related lncRNA was developed. Then, to further investigate the influence of m^{6}A-related lncRNAs on TIME, we deeply examined consensus clustering, risk model, immune checkpoints, immunoscore and immune cell infiltrating in ccRCC patients. This research also aims to provide insight on the underlying mechanisms and immunotherapeutic options that are involved in TIME.

Materials And Methods

Database

The Cancer Genome Atlas (TCGA, https://tcgadata.nci.nih.gov/tcga/) provided transcriptome profiling data in fragment per kilobase method (FPKM) format, as well as clinicopathological data for 539 ccRCC patients. On August 10, 2021, we gathered transcriptome data for 539 cases, comprising 539 ccRCC samples and 72 neighboring normal samples. The following were the criteria for inclusion: (1) Histology verified the presence of ccRCC. (2) m^{6}A regulator and lncRNA expression profiles and OS information were obtained at the same time. Clinicopathological data were available for 537 cases out of all cases, including age, gender, survival status, survival time, stage, TMN, grade, etc.

Bioinformatics analysis

Co-expression analysis of m^{6}A regulators and lncRNAs was used to find lncRNAs linked to m^{6}A. Univariate Cox analysis was performed between m^{6}A-related RNA expressions and overall survival using "survival" package to obtain m^{6}A-related lncRNAs with prognostic value. The "limma" program was used to compare the expression of m^{6}A-related lncRNAs in tumor and normal, and a heatmap was created. We utilized the "limma" program and the "Consusclusterplus" package (50 resampling, 80% resampling rate, Pearson) to split patients with ccRCC into distinct subtypes in order to functionally elucidate the biological properties of m^{6}A-related lncRNAs in ccRCC. Moreover, the "caret" program was used to randomly split 499 ccRCC patients into the training group (266 individuals) and testing group (264 individuals) in a 1:1 ratio. We used R v4.0.3 to evaluate the survival difference and construct the survival curve using the "survival" and "Survivminer" packages. Using gene set enrichment analysis (GSEA) v4.1.0, an enrichment analysis of the hallmark gene set "h.all.v7.4.symbols.gmt" and curated gene set "c2.cp.kegg.v7.4.symbols.gmt" of MsigDB was performed to show the various enriched biological processes or signaling pathways across distinct ccRCC subtypes, with 1000 premutation as the random sampling procedure.

The immunoscore of each patient was calculated using the "ESTIMATE" method. The immunoscore of 22 immune cell types in each sample was calculated with 1000 permutations by calculating relative subpopulations and cell type identification of RNA transcripts (CIBERPORT, https://cibersort.stanford.edu/). Only samples with $p < 0.05$ were kept for further analysis. These data were chosen to compare the degree of immune infiltration in cluster 1/2 and the high-/low-risk groups. The "Glmnet" program was used to perform LASSO regression analysis and 10-fold cross-validation to

determine the prognostic risk features of 30 m^6A-related lncRNAs. Using the coefficients of the LASSO regression approach, the risk score equation was created: risk score = sum of coefficients m^6A-related lncRNA expression level. The risk scores of each patient in the training cohort and testing cohort were determined using this algorithm. The patients were then separated into high-risk and low-risk groups using the median risk score as a dividing point.

Statistical analysis

For statistical tests, R version 4.0.3 was utilized. The Kaplan Meier procedure was used to create the survival curve, and the log rank test was utilized to examine the relationship between variables. Pearson correlation test was used to analyze the correlation between subtypes, clinic pathological features, risk scores, 5 immune checkpoints (CTLA4, TIGIT, PDCD1, CD19, LAG3) and immune infiltration levels. To investigate the independent predictive significance of risk scores associated with other clinical variables, the Cox regression model was employed for univariate and multivariate analysis. The prediction accuracy of m^6A-related lncRNAs for 1-, 3-, and 5-year OS was estimated using a ROC curve. It was statistically significant if the P value was less than 0.05.

Results

The co-expression network of m^6A regulators and lncRNAs was constructed to identify m^6A-related lncRNAs

From TCGA, m^6A-related gene expression data and clinical data of 539 ccRCC patients and 72 adjacent normal kidney specimens were obtained. The correlation test was carried out after extracting the expression of m^6A regulators and lncRNAs. Under the filter condition of corfilter = 0.4 and pvaluefilter = 0.001, 2243 lncRNAs were respectively regulated by 20 m^6A regulators, including 7 "writers" (METTL3, METTL14, METTL16, RBM15, RBM15B, VIRMA, ZC3H13), 11 "readers" (YTHD1/2, YTHDF2/3, HNRNPC, HNRNPA2B1, IGF2BP1/2, RBMS, FMR1, LRPPRC), and 2 "erasers" (ALKBH5, FTO). The co-expression network was then visualized in a network diagram using Cytoscape 3.8.2, with 2263 nodes and 4636 edges (**Fig. 1a**). For better visualization, we also set the conditions to corfilter = 0.6 and pvauluefilter = 0.01 to represent a higher correlation between 796 lncRNAs and 11 m^6A regulators (**Fig. 1b**).

m^6A-related lncRNAs was differentially expressed in ccRCC

For further analysis, the expression data of 2263 lncRNAs obtained with corfilter = 0.4 and pvaluefilter = 0.01 were retrieved. The top 30 most significant m^6A-related lncRNAs associated with prognosis were shown in the forest plot (**Fig. 2a**), heatmap (**Fig. 2b**), and box diagram (**Fig. 2c**). We compared the expression patterns of 30 prognostic m^6A-related lncRNAs across tumor and control groups in great detail. Twenty-eight m^6A-related lncRNAs were found to be highly expressed in the tumor group, including AC005841.1, AC012073.1, SNHG3, MED8-AS1, DGUOK-AS1, AC008870.2, LINC01355, RFPL3S, AP002807.1, AC016773.2, AC069281.2, VPS9D1-AS1, AC008105.1, CD27-AS1, AL451050.2, AL355388.1,

AL391244.2, AC005261.3, AC018648.1, AC005785.1, AC024060.2, AL139123.1, SCAT2, AC068620.2, AL662797.2, AC084876.1, AC095057.3 and AL354760.1. HOTAIRM1 and AC079174.2 were low expressed in the tumor group.

Survival and features of ccRCC patients are strongly linked to m^{6}A lncRNA consensus clustering

From k = 2 to 9, k = 2 was selected as best clustering stability according to the expression of the 30 m^{6}A-related lncRNAs and the fraction of ambiguous clustering (**Fig. 3a**). The 418 patients with ccRCC were categorized into two groups: cluster 1 (n = 418) and cluster 2 (n = 112). Cluster 2 had higher expression of 30 prognostic m^{6}A-related lncRNAs than cluster 1, with differences in clinicopathological features shown in **Fig. 3b**. Cluster 2 was characterized by G3-4, stage III-IV, T3-4, M1 and N1 ($p < 0.05$). Cluster 2 had a considerably higher immunoscore ($p < 0.05$) than cluster 1, while cluster 1 had a significantly longer overall survival (OS, $p < 0.001$) than cluster 2. (Fig. 3c).

The clustering subgroups described by m^{6}A-related lncRNAs were shown to be strongly connected to the heterogeneity of ccRCC patients, according to our findings. To investigate the m^{6}A-related lncRNAs, we examined the relationships between m^{6}A regulators and the aforementioned lncRNAs. LRPPRC was shown to be negatively connected with AL354760.1 and AC005261.3, and positively linked with AC069281.2, according to the findings. VIRMA was positively correlated with AC069281.2. RBM15 was positively correlated with DGUOK-AS1, AC011815.1 and LINC01355. METTL14 was positively correlated with AC011815.1. YTHDC2 was positively correlated with AC011815.1. FMR1 was positively correlated with AC011815.1. METTL3 was positively correlated with AC005841.1, AC024060.2, SNHG3, AL451050.2, AC012073.1, AC069281.2, AC084876.1CD27-AS1, AC008870.2, AL355388.1, AL139123.1, SCAT2, LINC01355, DGUOK-AS1, AL391244.2, AC016773.2, AC068620.2, AP002807.1, AC095057.3, AC079174.2, RFPL35, AC005785.1 and AL662797.2. HNRNPA2B1 was positively correlated with AC005785.1, AC008105.1, AC008870.2, AC012073.1, AC016773.2, AC018648.1, AC024060.2, AC068620.2, AC069281.2, AC079174.2, AC084876.1, AC095057.3, AL139123.1, AL355388.1, AL391244.2, AL451050.2, AL662797.2, AP002807.1, CD27-AS1, HOTAIRM1, RFPL3S, SCAT2, SNHG3, VPS9D1-AS1, LINC01355 and DGUOK-AS1. (**Fig. 3d**)

Association between immune checkpoints and m^{6}A-related lncRNAs

To investigate the relationship between immune checkpoints and m^{6}A-related lncRNAs and their impact on ccRCC prognosis, we first examined the expression of CTLA4, TIGIT, PDCD1, CD19, and LAG3 in tumor/normal, cluster 1/2, and high-/low-risk groups, and then used Pearson correlation method to examine the interactions in both immune checkpoints and 30 prognostic m^{6}A-related lncRNAs. In the cluster 2, high-risk, and tumor groups, CTLA4, TIGIT, PDCD1, CD19, and LAG3 were all significantly overexpressed, as shown in **Fig. 4a-e**, and these proteins were found to be strongly associated with the lncRNAs previously described.

A Pearson correlation analysis was utilized to examine the association between the 5 immune checkpoints and the 30 prognostic lncRNAs, which included HOTAIRM1, CD27-AS1, AL662797.2, AC016773.2, AC012073.1, AL451050.2, AC095057.3, AC024060.2, AC018648.1, AC008870.2, AC084876.1, AP002807.1, LINC01355, AC079174.2, AC005261.3, AC069281.2, AC005785.1, AL355388.1, DGUOK-AS1, AL354760.1, SNHG3, VPS9D1-AS1, AC005841.1, AC008105.1, MED8-AS1, RFPL3S, AL391244.2, SCAT2 and AC068620.2. CTLA4 was positively correlated with the abovementioned 30 lncRNAs. TIGIT, as well as PDCD1 and LAG3, were positively linked with 29 of the 30 lncRNAs except AC018648.1. CD19 was positively correlated with all 26 lncRNAs except CD27-AS1, AL139123.1, AL391244.2 and AC068620.2. (**Fig. 4f**)

Interactions of immune cell infiltration with clustering based on m^{6}A-related lncRNAs

To investigate the influence of clustering based on m^{6}A-related lncRNAs on TIME, we compared the immunoscore and immune cell infiltration between cluster 1 which had elevated lncRNAs and cluster 2 which had down-regulated lncRNAs. Cluster 2 had a much higher immunoscore than cluster 1, which was a meaningful difference. Overall survival in cluster 2 was, however, lower than in cluster 1 (**Fig. 5a**), indicating a more serious condition in cluster 2. Following that, the percentage of 22 immune cell types across the two clusters was compared to see which one was more prevalent (**Fig. 5k**). M1 macrophages ($p < 0.01$), M2 macrophages ($p < 0.001$), resting mast cells ($p < 0.01$), resting memory CD4$^+$ T cells ($p < 0.001$), and naive B cells ($p < 0.05$) were all found in larger numbers in cluster 1 (**Fig. 5b-f**). Cluster 2 had greater infiltration of activated NK cells ($p < 0.05$), CD8$^+$ T cells ($p < 0.01$), regulatory T cells (Tregs, $p < 0.001$), and follicular helper T cells ($p < 0.001$) (**Fig. 5g-j**). We used GSEA to determine the probable regulatory mechanisms underlying the difference in TIME between the 2 clusters. The findings revealed that the tumor's malignant features included protein secretion [normalized enrichment score (NES) = -2.33, $p < 0.001$, FDR = 0.004], androgen response (NES = -2.30, $p < 0.001$, FDR = 0.003), adipogenesis (NES = -2.24, $p < 0.001$, FDR = 0.004), bile acid metabolism (NES = -2.30, $p < 0.001$, FDR = 0.003), fat acid metabolism (NES = -2.30, $p < 0.001$, FDR = 0.003), PPAR signaling pathway (NES = -1.89, $p < 0.01$, FDR < 0.05) and ErbB signaling pathway (NES = -2.13, $p < 0.05$, FDR < 0.05) (**Fig. 6**). TIME variation between cluster 1 and 2 might be attributed to these signaling pathways.

Construction and validation of m^{6}A-related lncRNAs prognostic signal

In ccRCC patients, we studied the function of lncRNAs as prognostic factor. The 530 patients were randomly split into two groups on random: the training cohort (266 cases) and the testing cohort (264 cases). There was no significant difference between training cohort and testing cohort in terms of age, gender, T stage, M stage, N stage and grade ($p > 0.05$). LASSO regression analysis was conducted on 30 prognostic m^{6}A-related lncRNAs expressed in the training cohort to successfully predict ccRCC patients' clinical outcomes. Then, the 6 lncRNAs with the most stable changes in tumors were obtained, namely AC012073.1, AC084876.1, AC005261.3, AL355388.1, AC005841.1 and AL391244.2. For both the training

cohort and the testing cohort, the coefficient generated by the LASSO algorithm was utilized to calculate the risk score. The following was the formula: risk score = sum of coefficients × level of m^6A-related lncRNA expression. The patients were then separated into two groups based on their median risk score: high-risk and low-risk groups. The risk score, OS overall survival, OS status, and expression profiles of the discovered risk signatures (AC012073.1, AC084876.1, AC005261.3, AL355388.1, AC005841.1, and AL391244.2) in the training and testing cohorts were calculated using the expression levels and coefficients of the 6 lncRNAs (**Fig. 9a, 9b**). Six lncRNAs showed their expressions increased in the high-risk group. The low-risk group's OS was longer than the high-risk group's OS in both the training and testing cohorts ($p < 0.001$, **Fig. 9a, 9b**). We evaluated the area under the curve (AUC) of the 1-, 3-, and 5-year ROC curves to assess the predictive accuracy of the 6 risk signatures found (**Fig. 8**). The AUC of 6 risk indicators at 1, 3, and 5 years in the training cohort was 0.721, 0.662, and 0.752, respectively, while the AUC of the 6 risk characteristics at 1, 3, and 5 years in the testing cohort was 0.653, 0.667, and 0.691, indicating that the risk indicators of 6 lncRNAs had good differential performance for the prognosis of ccRCC patients. Patients with ccRCC may benefit from calculating a risk score based on six risk signatures, according to these findings.

A connection exists between ccRCC risk scores and a variety of clinical indicators

A closer analysis at the link between risk scores and clinical features was conducted. The heatmap depicted the expression patterns of six lncRNAs in the training cohort's high- and low-risk groups. In the high-risk group, the expression of AC012073.1, AC084876.1, AC005261.3, AL355388.1, AC005841.1, and AL391244.2 was increased. As shown in **Fig. 11**, the risk ratings were very different in clusters ($p < 0.001$), grade ($p < 0.01$), stage ($p < 0.001$), T (($p < 0.001$), and M stage ($p < 0.05$). Cluster 2 has a considerably higher risk score than cluster 1 ($p < 0.001$, **Fig. 12a)**. Groups with a higher immunoscore had higher risk scores ($p < 0.001$, **Fig. 12b**). Risk scores increased with rising of grade ($p < 0.001$, **Fig. 12c**), T ($p < 0.001$, **Fig. 12d**), M ($p < 0.001$, **Fig. 12e**), and stage ($p < 0.001$, **Fig. 12f)**. These results suggested that risk scores in patients with ccRCC were significantly correlated with the clusters, grade, stage, and immunoscores. Finally, we conducted model validation of clinical grouping, and the results suggested that the risk model was suitable for male, female, ≥65 years old, ≤65 years old, G1-2, G3-4, T1-2, T3-4, M0, N0, stage I-II, stage III-IV patients (**Fig. 13**, $p < 0.001$).

Infiltration of immune cells by m^6A-related lncRNA

There were 22 immune cell types that were studied to see if the risk model had an effect on the TIME. A higher risk score was linked to higher levels of activated NK cells ($p < 0.05$), memory B cells ($p < 0.05$), $CD8^+$ T cells ($p < 0.001$), follicular helper T cells ($p < 0.001$), and Tregs ($p < 0.001$), while lower risk scores were linked to lower levels of activated B cells ($p < 0.001$), activated dendritic cells ($p < 0.001$), resting dendritic cells ($p < 0.001$), resting memory $CD4^+$ T cells ($p < 0.05$), M2 macrophages ($p < 0.001$), resting mast cells ($p < 0.001$) and neutrophils ($p < 0.001$), as shown in the **Fig. 14**. This finding indicated that the

risk score derived from m^{6}A-related lncRNAs is dependent on TIME, with a variable TIME resulting in a different risk score for ccRCC patients.

Discussion

As the most common subtype of renal cell carcinoma, ccRCC has attracted the attention of many investigators who want to learn more about its pathogenesis and treatment. Diverse clusters of multiple malignancies, including ccRCC, can exhibit different clinical features and treatment outcomes because of heterogeneity in histology and gene expression. Due to tumor heterogeneity, different situations of the same type of tumor should require different immunotherapy strategies, which brings numerous challenges to successful tumor treatment. Searching for the different clusters based on meaningful mediators is therefore critical for tumor therapy. Herein, m^{6}A-related lncRNAs have been used to construct diverse molecular subtypes for ccRCC by consensus clustering as a novel determinant in the TIME. In our study, we have performed a comprehensive investigation of the relationship between m^{6}A-related lncRNAs, immune checkpoints, immune cell infiltrations, and different clinical outcomes in ccRCC patients.

Posttranscriptional modifications such as m^{6}A are the most prevalent post-transcriptional modifications in Eukaryotic nucleic acids (mRNAs) and non-nucleic acids (lncRNAs). As competing endogenous RNAs, LncRNAs may alter tumor invasion and progression [20], including that of ccRCC [5, 6], by targeting the m^{6}A regulator. By providing binding sites for m^{6}A reader proteins, m^{6}A alteration may influence lncRNA function [17, 19, 20, 21]. However, it's not yet clear what the role of m^{6}A lncRNAs in the etiology and prognosis of ccRCC is. Because of this, we attempted to build a new model using the m^{6}A-related lncRNAs.

In this work, a total of 2243 m^{6}A-related lncRNAs identified from TCGA have been studied for their prognostic value. A univariate Cox regression analysis demonstrated that lncRNAs associated to m^{6}A were the most significant risk factor, supporting the prognostic significance of 30 lncRNAs associated to m^{6}A. SNHG3 and HOTAIRM1 have been studied in ccRCC [22–23], while the others, such as GUOK-AS1, LINC01355, VPS9D1-AS1, and CD27-AS1, have been studied in a variety of cancers [22–26]. SNHG3 has the potential to increase the proliferation and spread of ccRCC cells [22]. The hypoxia pathway can be inhibited by HOTAIRM1, which is downregulated in ccRCC [23]. In acute myeloid leukemia, downregulation of CD27-AS1 reduces cancer cell growth, causes cells to stagnate in the G0/G1 phase, and triggers apoptosis [26].

Based on 30 prognostic lncRNAs associated to m^{6}A, all patients were classified into two clusters: cluster 1 and cluster 2. Cluster 2 had a considerably higher immunoscore and immune cell infiltration than cluster 1, which was followed by a poor prognosis and clinical outcome. Based on the medium risk score, ccRCC patients were classified into high-risk and low-risk groups, respectively. The clinical outcomes of the high-risk group were much poorer. The risk model was applicable to patients with diverse clinical

characteristics, including men and females, > 65 years old, 65 years old, G1-2, G3-4, T1-2, T3-4, M0, N0, Stage I-II, and Stage III-IV, according to survival studies based on various clinical features. This further validates the risk model's accuracy. The observed and anticipated rates of 1-, 3-, and 5-year OS were perfectly consistent in our survival analysis curve. Finally, the observed agreement with the 1-, 3-, and 5-year prediction rates was outstanding. The risk model, which is based on six m^6A-related lncRNAs that are all independently linked to OS, is highly accurate. This prediction model may help identify additional biomarkers in future research.

To explain the difference in survival between cluster 1/2 and high-/low-risk groups, we investigated at the function of TIME in ccRCC. Activated NK cells, $CD8^+$ T cells, follicular helper T cells, and Tregs, all of which were substantially expressed in Cluster 2 and were associated with extended overall survival, also had a favorable relationship with the risk score. Cluster 1 showed significant levels of M2 macrophages, resting mast cells, naïve B cells, and resting memory $CD4^+$ T cells, all of which had a negative connection with overall survival. Our findings suggest that activated NK cells, $CD8^+$ T cells, follicular helper T cells, and Tregs may aid in the development of ccRCC, resulting in a poor patient prognosis. M2 macrophages, resting mast cells, naive B cells, and resting memory $CD4^+$ T cells, on the other hand, may slow the advancement of ccRCC, resulting in a favorable outcome.

Different levels of immune checkpoint and immune cell filtration might explain the significant difference in survival between the two risk groups. Cluster 2 and high-risk patients had higher immunoscores, suggesting that patients with high immunoscores are more likely to have a bad prognosis and a short survival period. Cluster 2, tumor group, and high-risk group had greater CTLA4, TIGIT, CD19, PDCD1, and LAG3 expression than cluster 1, normal group, and low-risk group, which linked to a higher immunoscore, poor overall survival rate, and prognosis. These findings are mostly in line with those of prior studies [16, 27–29]. CTLA4, CD274, PDCD1, PDCD1LG2, HAVCR2, TIGIT, and LAG3 were reported to be elevated and might trigger cell apoptosis in ccRCC by Liao et al [16]. In ccRCC patients, CTLA4 expression was positively linked to 22 immune cells, and patients with high CTLA4 expression had shorter survival times, as previously shown [14, 13, 30]. Targeting immune checkpoints has been one of the most successful treatments for malignant tumors in recent years [15, 31–34]. One of these is anti-CTLA4 immunotherapy, which has been demonstrated to be effective in the treatment of ccRCC [15]. The therapeutic value of the other four immune checkpoint antibodies has not been described in ccRCC but has been reported in other malignancies. Anti-TIGIT [31], anti-CD19 [32], anti-PDCD1 [33], and anti-LAG3 [34] immunotherapy, for example, have been shown to successfully slow the development of soft tissue sarcoma [31], acute lymphoblastic leukemia [32], central nervous system lymphoma [33], and multiple myeloma [34]. The expression of 30 lncRNAs and 5 immune checkpoints differed across clusters 1 and 2, as well as between high-risk and low-risk groups, implying that they may greatly affect clinical outcomes in ccRCC.

According to the GSEA results, the 6 m^6A-related lncRNAs may be the key factors causing different TIME via various biological processes or signaling pathways such as protein secretion, androgen response, adipogenesis, bile acid metabolism, fatty acid metabolism, PPAR signaling pathway, and ErbB signaling

pathway. As a result, these biological processes and signal pathways could be implicated in various TIME. The enhanced expression of the androgen receptor (AR) is associated with tumor angiogenesis. AR stimulates the creation of angiogenic mimics in ccRCC cells by modulating the lncRNA TANAR/TWIST1 pathway, according to in vitro studies [35]. By inhibiting angiogenesis, the AR/TANA/TWIST1 pathway can slow the advancement of ccRCC. The adipocyte-like morphology of ccRCC is determined by grade-dependent neutral lipid accumulation in cells [36]. Shen et al. discovered that SREBP1-dependent fatty acid production promotes ccRCC proliferation and metastasis [24]. By modulating glucose homeostasis and lipid metabolism death, PPAR may contribute to increased E-cadherin, leading in suppression of tumor cell migration and proliferation. [37]. Inhibiting m^6A methylation by knocking down METTL3 can reduce PPAR m6A abundance and lengthen PPAR mRNA longevity and expression, minimizing lipid accumulation. ErbB phosphorylation or increased ErbB expression can inhibit the development of ccRCC cells [38]. These results suggest that m^6A-related lncRNA regulate the TIME between the two clusters by acting on androgen response, lipogenesis, fatty acid metabolism, PPAR signal pathway, and ErbB signal pathway.

Immunotherapy targeting TIME is a promising treatment for ccRCC. In our research, we discovered that the m^6A-related lncRNA may regulate the TIME by modulating immune cell infiltration or immune checkpoints, resulting in various tumor progression phases and clinical outcomes. Across the whole process, no matter targeting any part, such as m^6A regulators, lncRNA, the level of immune cell infiltration, or immune markers, it is possible to change the condition of TIME, so as to prevent the occurrence and development of ccRCC, as well as to treat ccRCC or improve the prognosis of the patients.

There is no denying that our study has some limitations. First, the mentioned risk scoring model and the interaction between TIME and m^6A-related lncRNAs have not been externally verified. Second, we haven't collected the transcriptome data of m^6A regulators and lncRNAs of ccRCC patients in our apartment. Therefore, we will obtain the sequencing cases of our hospital in the future to improve the prediction model. Meanwhile, further experiments in vivo or in vitro were required to verify the specific regulatory mechanism of m^6A-related lncRNAs in ccRCC.

Conclusions

This work developed a predictive signature based on m^6A-related lncRNAs and assessed its significance in the TIME of ccRCC patients. These lncRNAs might be potential targets for accurate diagnosis and immunotherapy in patients with ccRCC. With poor clinical outcomes, patients in cluster 2 and high-risk had higher levels of CTLA4, TIGIT, CD19, LAG3, and PDCD2. They affect the TIME by controlling immune checkpoints and immune cell infiltration, which affects the immunoscore of ccRCC. There was a clear positive connection between 30 m^6A-related lncRNAs associated and immune checkpoints. In other words, higher immunoscores and the 5 immune checkpoints indicate worse prognosis for ccRCC patients. High risk scores are associated with upregulated immune cell infiltrates such as activated NK cells, memory B cells, $CD8^+$ T cells, follicular helper T cells, and Treg infiltration and downregulated

immune cell infiltrates such as activated B cells, activated dendritic cells, resting cells, resting memory $CD4^+$ T cells, M2 macrophages, resting mast cells, and neutrophils. All of the aforementioned linked relationships are ultimately reliant on m^6A-related lncRNA, whether via androgen response, lipogenesis, fatty acid metabolism, the PPAR signal pathway, or the ErbB signal pathway. It may be possible to improve the immunotherapy response of ccRCC by identifying the molecular pathways that influence the immune response.

Abbreviations

RCC: Renal cell carcinoma; ccRCC: Clear cell renal cell carcinoma; LncRNA: Long noncoding RNA; m^6A: N^6 Methyladenosine; TIME: Tumor immune microenvironment; FPKM: Fragment per kilobase method; TCGA: The Cancer Genome Atlas; GSEA: Gene set enrichment analysis; AUC: Area under the curve; OS: Overall survival; ES: Enrichment score; NES: Normalized ES; NOM p-value: Normalized p-value

Declarations

Ethics approval and consent to participate

Not applicable.

Consent for publish

Not applicable.

Availability of data and materials

The data was obtained from TCGA data portal (https://portal.gdc.cancer.gov/projects/TCGA-KIRC). The authors did not have special access privileges.

Competing interests

The authors declare that they have no competing interests.

Funding

This work was supported by Fund Program for the Scientific Activities of Selected Returned Overseas Professionals in Shanxi Province (2017-29) and Research Project Supported by Shanxi Scholarship Council of China (2020-186).

Authors' Contributions

LH and QX designed the study; LH, WL, ZJ and GX carried out data collection; LH performed data analysis and wrote the paper; QX contributed analytic tools and revised the paper. All authors have read and approved the final manuscript.

Acknowledgements

Not applicable.

References

1. Miller KD, Nogueira L, Mariotto AB, et al. Cancer treatment and survivorship statistics. CA Cancer J Clin. 2019;69:363-385.
2. Hsieh JJ, Purdue MP, Signoretti S, et al. Renal cell carcinoma. Nat Rev Dis Primers. 2017;3:17009.
3. Hahne JC, Valeri N. Non-Coding RNAs and Resistance to Anticancer Drugs in Gastrointestinal Tumors. Front Oncol. 2018;8:226.
4. Mohapatra S, Pioppini C, Ozpolat B, et al. Non-coding RNAs regulation of macrophage polarization in cancer. Mol Cancer. 2021;20:24.
5. Gu Y, Niu S, Wang Y, et al. DMDRMR-Mediated Regulation of mA-Modified by mA Reader IGF2BP3 Drives ccRCC Progression. Cancer Res. 2021;81:923-934.
6. Qiu Y, Wang X, Fan Z, et al. Integrated analysis on the N6-methyladenosine-related long noncoding RNAs prognostic signature, immune checkpoints, and immune cell infiltration in clear cell renal cell carcinoma. Immun Inflamm Dis. 2021. doi:10.1002/iid3.513.
7. Huang W, Chen TQ, Fang K, et al. N6-methyladenosine methyltransferases: functions, regulation, and clinical potential. J Hematol Oncol. 2021;14:117.
8. Wen S, Wei Y, Zen C, et al. Long non-coding RNA NEAT1 promotes bone metastasis of prostate cancer through N6-methyladenosine. Mol Cancer. 2020;19:171.
9. Wang Y, Lu JH, Wu QN, et al. LncRNA LINRIS stabilizes IGF2BP2 and promotes the aerobic glycolysis in colorectal cancer. Mol Cancer. 2019;18:174.
10. Zhang S, Zhang E, Long J, et al. Immune infiltration in renal cell carcinoma. Cancer Sci. 2019;110:1564-1572.
11. Bai D, Feng H, Yang J, et al. Genomic analysis uncovers prognostic and immunogenic characteristics of ferroptosis for clear cell renal cell carcinoma. Mol Ther Nucleic Acids. 2021;25:186-197.
12. Kamai T, Kijima T, Tsuzuki T, et al. Increased expression of adenosine 2A receptors in metastatic renal cell carcinoma is associated with poorer response to anti-vascular endothelial growth factor agents and anti-PD-1/Anti-CTLA4 antibodies and shorter survival. Cancer Immunol Immunother. 2021;70:2009-2021.
13. Min L, Vaidya A, Becker C. Thyroid autoimmunity and ophthalmopathy related to melanoma biological therapy. Eur J Endocrinol. 2011;164:303-7.
14. Liu S, Wang F, Tan W, et al. CTLA4 has a profound impact on the landscape of tumor-infiltrating lymphocytes with a high prognosis value in clear cell renal cell carcinoma (ccRCC). Cancer Cell Int. 2020;20:519.

15. Klümper N, Ralser DJ, Zarbl R, et al. CTLA4 promoter hypomethylation is a negative prognostic biomarker at initial diagnosis but predicts response and favorable outcome to anti-PD-1 based immunotherapy in clear cell renal cell carcinoma. J Immunother Cancer. 2021;9(8):e002949.
16. Liao G, Wang P, Wang Y. Identification of the Prognosis Value and Potential Mechanism of Immune Checkpoints in Renal Clear Cell Carcinoma Microenvironment. Front Oncol. 2021;11:720125.
17. Zhang X, Shen L, Cai R, et al. Comprehensive Analysis of the Immune-Oncology Targets and Immune Infiltrates of N^6-Methyladenosine-Related Long Noncoding RNA Regulators in Breast Cancer. Front Cell Dev Biol. 2021;9:686675.
18. Qian X, Yang J, Qiu Q, et al. LCAT3, a novel m6A-regulated long non-coding RNA, plays an oncogenic role in lung cancer via binding with FUBP1 to activate c-MYC. J Hematol Oncol. 2021;14:112.
19. Xu F, Huang X, Li Y, et al. mA-related lncRNAs are potential biomarkers for predicting prognoses and immune responses in patients with LUAD. Mol Ther Nucleic Acids. 2021;24:780-791.
20. Zhou KI, Parisien M, Dai Q, et al. N(6)-Methyladenosine Modification in a Long Noncoding RNA Hairpin Predisposes Its Conformation to Protein Binding. J Mol Biol. 2016;428:822-833.
21. Chen Y, Lin Y, Shu Y, et al. Interaction between N-methyladenosine (mA) modification and noncoding RNAs in cancer. Mol Cancer. 2020;19:94.
22. Zhang C, Qu Y, Xiao H, et al. LncRNA SNHG3 promotes clear cell renal cell carcinoma proliferation and migration by upregulating TOP2A. Exp Cell Res. 2019;384:111595.
23. Hamilton MJ,Young M, Jang K, et al. HOTAIRM1 lncRNA is downregulated in clear cell renal cell carcinoma and inhibits the hypoxia pathway. Cancer Lett. 2020;472:50-58.
24. Wu N, Song H, Ren Y, et al. DGUOK-AS1 promotes cell proliferation in cervical cancer via acting as a ceRNA of miR-653-5p. Cell Biochem Funct. 2020;38:870-879.
25. Ai B, Kong X, Wang X, et al. LINC01355 suppresses breast cancer growth through FOXO3-mediated transcriptional repression of CCND1. Cell Death Dis. 2019;10:502.
26. Tao Y, Zhang J, Chen L, et al. LncRNA CD27-AS1 promotes acute myeloid leukemia progression through the miR-224-5p/PBX3 signaling circuit. Cell Death Dis. 2021;12:510.
27. Dai S, Zeng H, Liu Z, et al. Intratumoral CXCL13CD8T cell infiltration determines poor clinical outcomes and immunoevasive contexture in patients with clear cell renal cell carcinoma. J Immunother Cancer. 2021;9:e001823.
28. Hua X, Chen J, Su Y, et al. Identification of an immune-related risk signature for predicting prognosis in clear cell renal cell carcinoma. Aging (Albany NY). 2020;12:2302-2332.
29. Wan B, Liu B, Huang Y, et al. Identification of genes of prognostic value in the ccRCC microenvironment from TCGA database. Mol Genet Genomic Med. 2020;8:e1159.
30. Xiao GF, Yan X, Chen Z, et al. Identification of a Novel Immune-Related Prognostic Biomarker and Small-Molecule Drugs in Clear Cell Renal Cell Carcinoma (ccRCC) by a Merged Microarray-Acquired Dataset and TCGA Database. Front Genet. 2020;11:810.

31. Judge SJ, Darrow MA, Thorpe SW, et al. Analysis of tumor-infiltrating NK and T cells highlights IL-15 stimulation and TIGIT blockade as a combination immunotherapy strategy for soft tissue sarcomas. J Immunother Cance. 2020;8(2):e001355.
32. Viardot A, Sala E. Investigational immunotherapy targeting CD19 for the treatment of acute lymphoblastic leukemia. Expert Opin Investig Drugs. 2021;30:773-784.
33. Qiu Y, Li Z, Pouzoulet F, et al. Immune checkpoint inhibition by anti-PDCD1 (anti-PD1) monoclonal antibody has significant therapeutic activity against central nervous system lymphoma in an immunocompetent preclinical model. Br J Haematol. 2018;183:674-678.
34. Bae J, Accardi F, Hideshima T, et al. Targeting LAG3/GAL-3 to overcome immunosuppression and enhance anti-tumor immune responses in multiple myeloma. Leukemia. 2021. doi:10.1038/s41375-021-01301-6.
35. You B, Sun Y, Luo J, et al. Androgen receptor promotes renal cell carcinoma (RCC) vasculogenic mimicry (VM) via altering TWIST1 nonsense-mediated decay through lncRNA-TANAR. Oncogene. 2021;40:1674-1689.
36. Bombelli S, Torsello B, De Marco S, et al. 36-kDa Annexin A3 Isoform Negatively Modulates Lipid Storage in Clear Cell Renal Cell Carcinoma Cells. Am J Pathol. 2020;190:2317-2326.
37. Wu Y, Song T, Liu M, et al. PPARG Negatively Modulates in Tumor Formation of Clear Cell Renal Cell Carcinoma. DNA Cell Biol. 2019;38:700-707.
38. Campion CG, Zaoui K, Verissimo T, et al. COMMD5/HCaRG Hooks Endosomes on Cytoskeleton and Coordinates EGFR Trafficking. Cell Rep. 2018;24:670-684.e7.

Figures

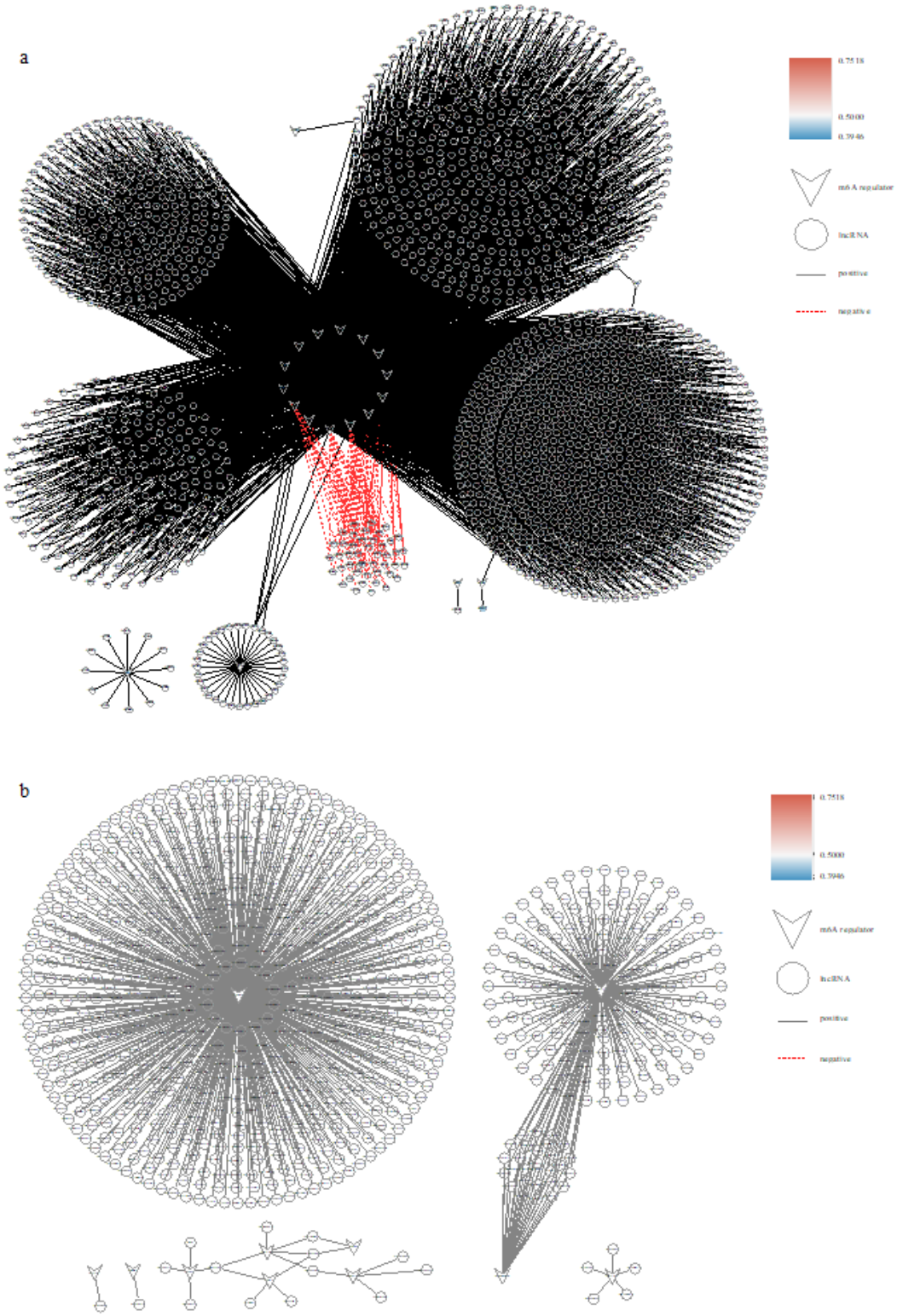

Figure 1

m^{6}A-lncRNA co-expression network. (a) The m^{6}A-lncRNA co-expression network under the filtering condition of corfilter = 0.4 and pvaluefilter = 0.001. It consists of 2263 nodes and 4636 edges. (b) The m^{6}A-lncRNA co-expression network under the filtering condition of corfilter = 0.6 and pvauluefilter = 0.01, consisting of 807 nodes and 827 edges.

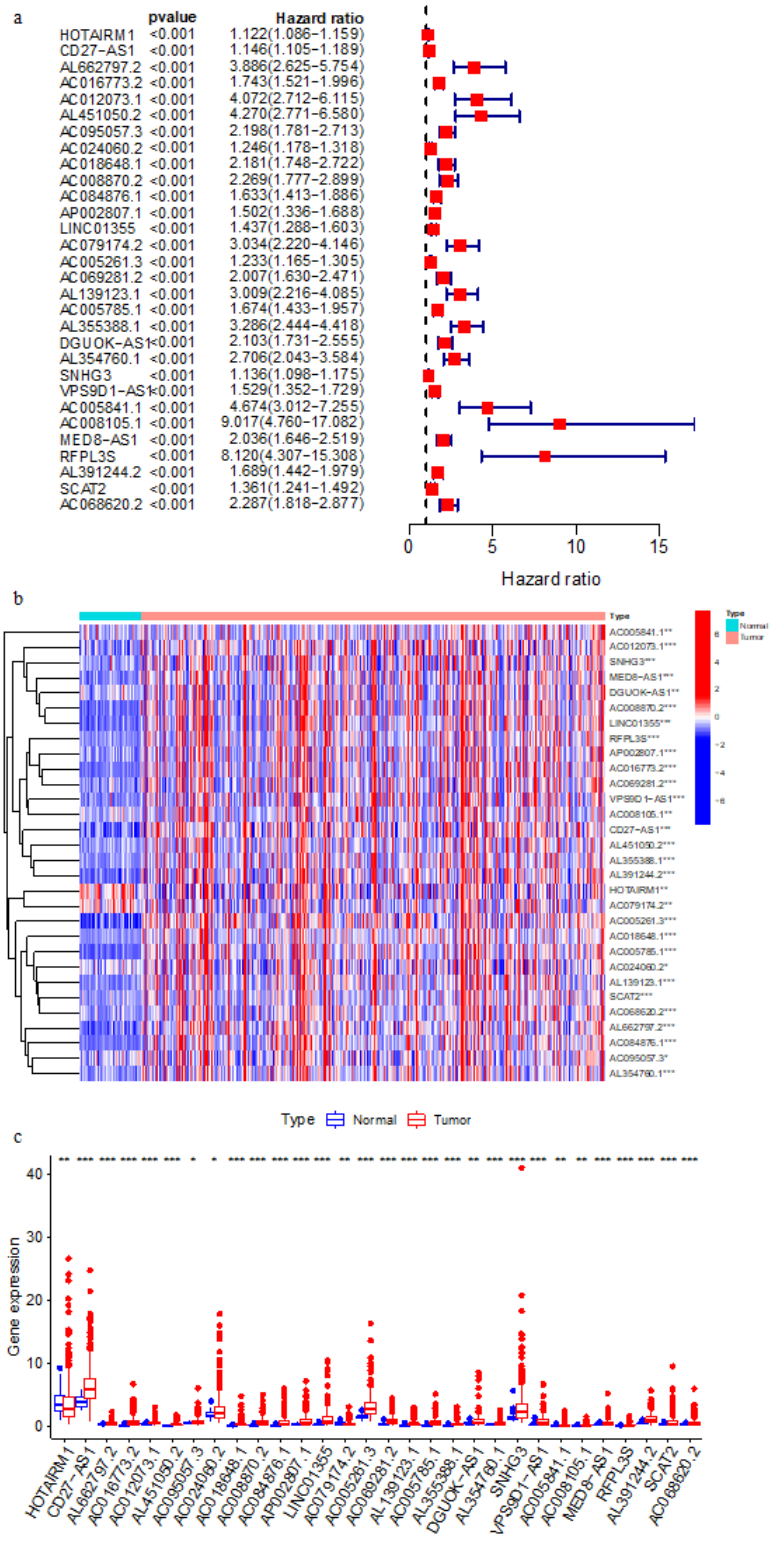

Figure 2

(a) After univariate regression analysis, 30 prognostic lncRNAs were identified. (b and c) Heatmap and boxplot that showed the expressions of 30 m^{6}A-related lncRNAs between tumors ** p< 0.05. ** p < 0.01. *** p< 0.001.

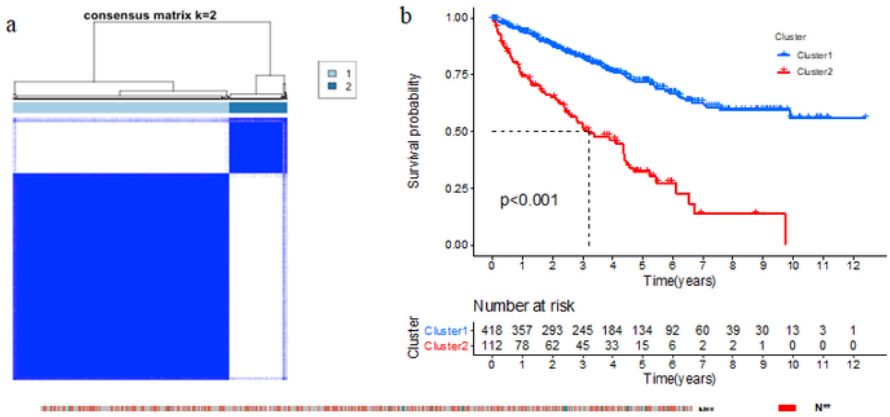

Figure 3

Differences in clinical and pathological characteristics and survival rates between the two clusters. (a) Clustering matrix with k = 2 that are approved on. (b) Kaplan-Meier curves of overall survival (OS) in two clusters. (c) Heatmap illustrating expressions of m^6A-related lncRNAsand clinicopathologic features in cluster 1/2. (d) The interaction among both m^6A regulators and the 30 prognostic m^6A-related lncRNAs. *p < 0.05 and **p< 0.01

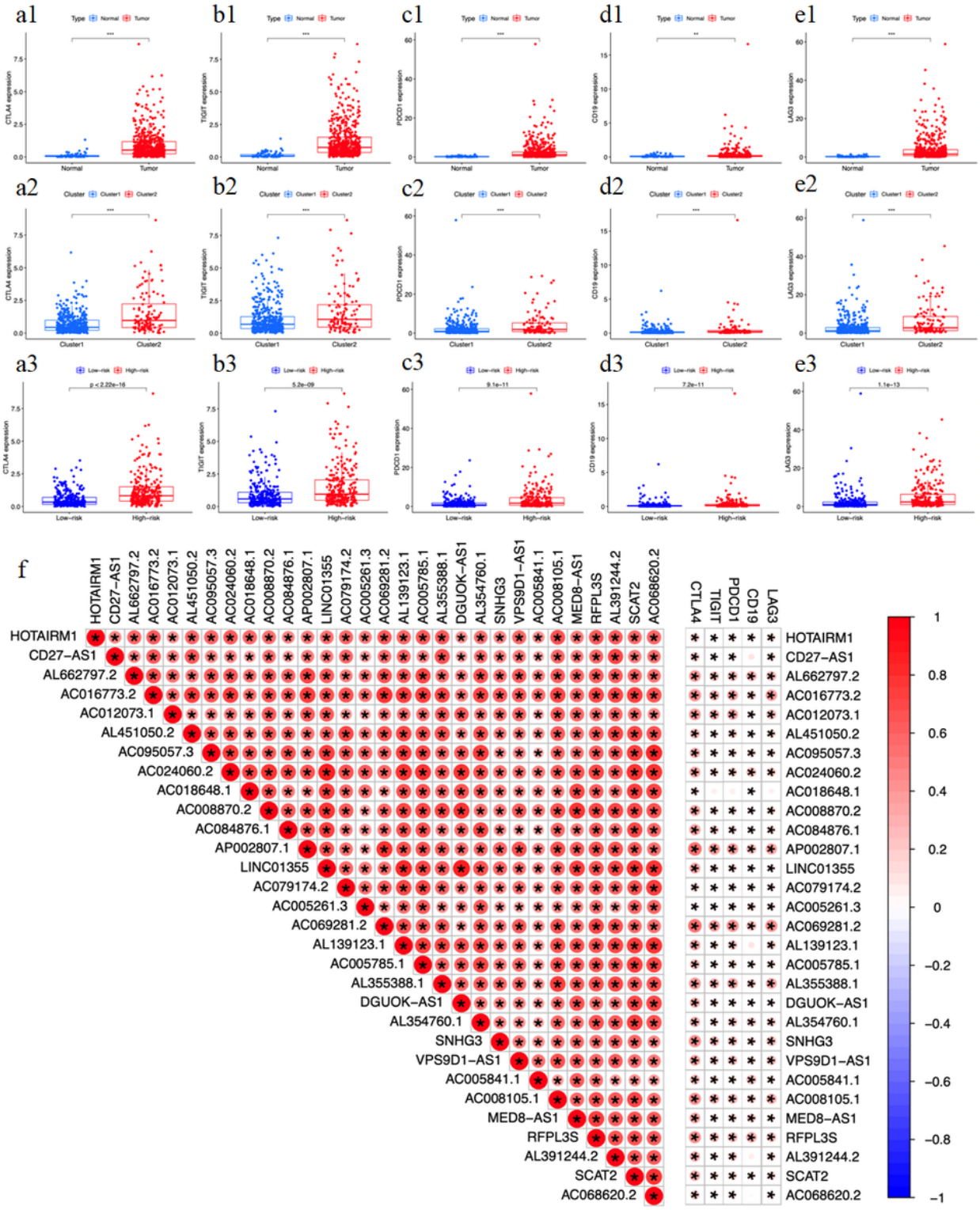

Figure 4

Association of 5 immune checkponits with m^{6}A-related lncRNAs and the landscape of immune cell infiltration in ccRCC. (a) CTLA4 upregulation in ccRCC (a1), cluster 1/2 (a2) and high-/low-risk groups (a3). (b) TIGIT upregulation in ccRCC (b1), cluster 1/2 (b2) and high-/low-risk groups (b3). (c) PDCD1 upregulation in ccRCC (c1), cluster 1/2 (c2) and high-/low-risk groups (c3). (d) CD19 upregulation in ccRCC (d1), cluster 1/2 (d2) and high-/low-risk groups (d3). (e) LAG3 upregulation in ccRCC (e1), cluster

1/2 (e2) and high-/low-risk groups (e3). (f) The correlation of CTLA4, TIGIT, PDCD1, CD19 and LAG3 with m^6A methylation regulators. *$p < 0.05$, **$p < 0.01$ and ***$p < 0.001$.

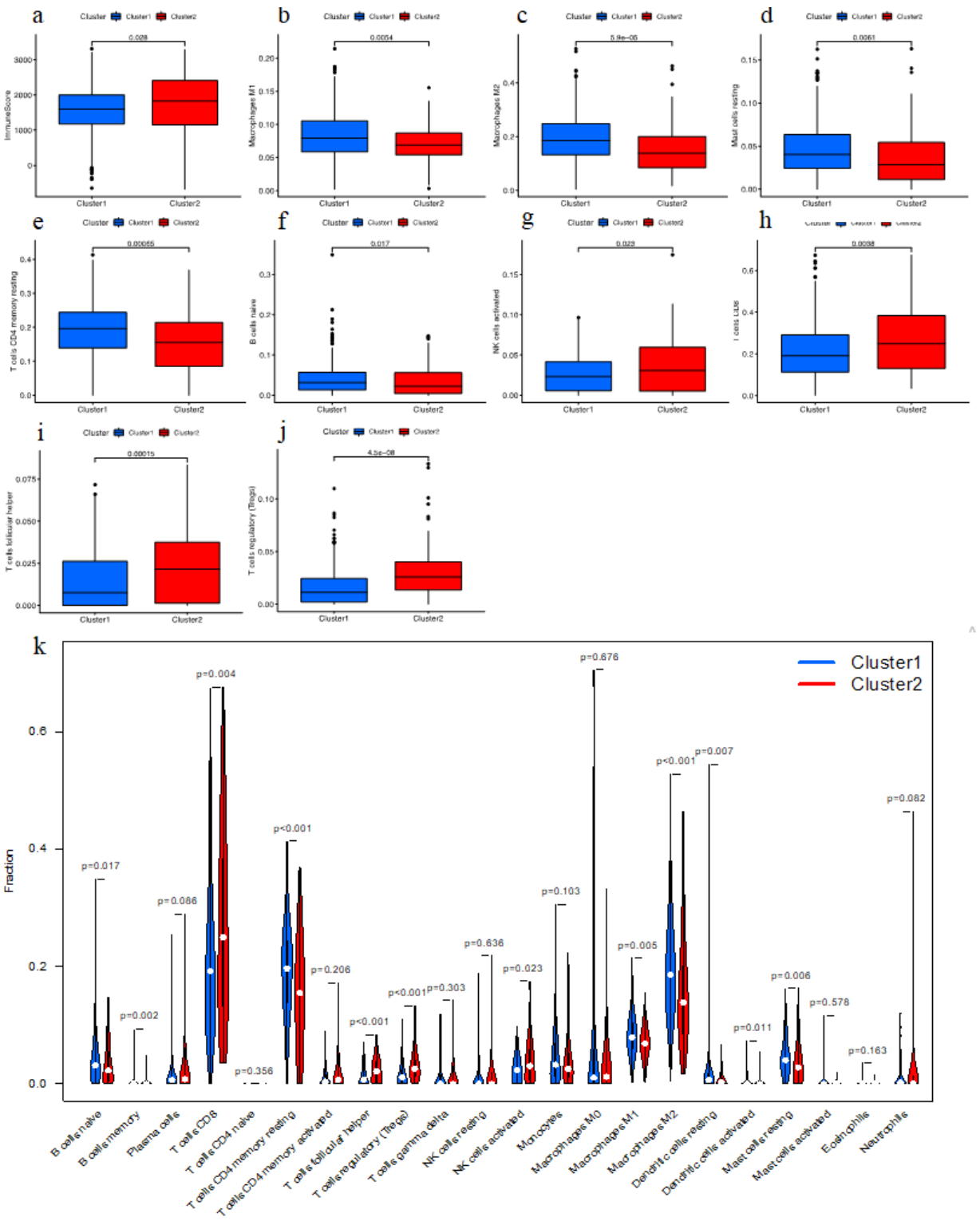

Figure 5

Different immune cell infiltration in two clusters. (a) Immune score in the cluster 1/2 subtypes. (b–j) The infiltrating levels of the M1 macrophage (b), M2 macrophage (c), resting mast cells (d), resting memory $CD4^+$ T cells (e), naive B cells (f), activated NK cells (g), $CD8^+$ T cells (h), follicular helper T cells (i) and regulatory T cells (j) and in two clusters. (k) The levels of infiltration of 22 immune cell types in 2 clusters.

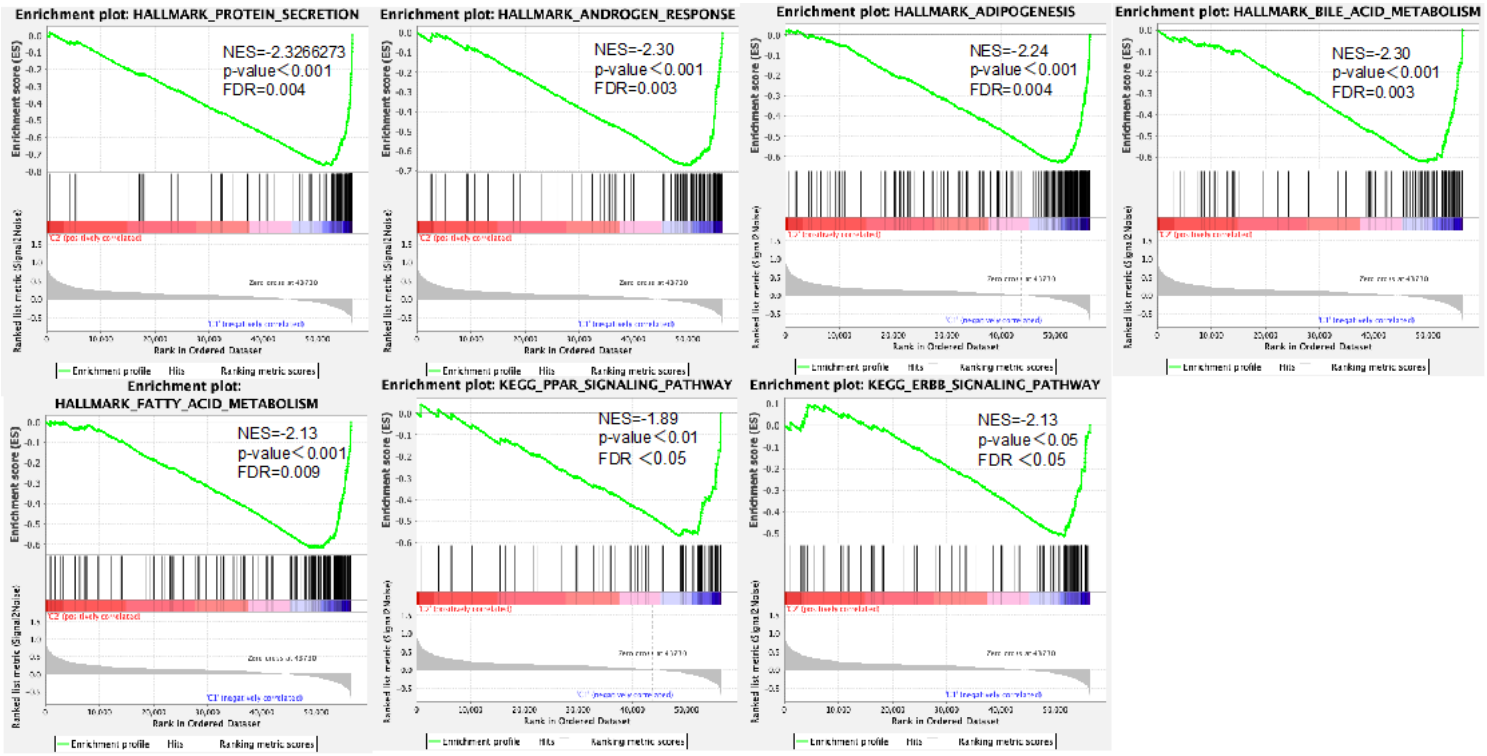

Figure 6

Gene set enrichment analysis (GSEA). Cluster 1 had significantly enriched protein secretion, androgen response, adipogenesis, bile acid metabolism, fat acid metabolism, PPAR signaling pathway, and ErbB signaling pathway. ES, enrichment score; NES, normalized ES; NOM p-value, normalized p-value.

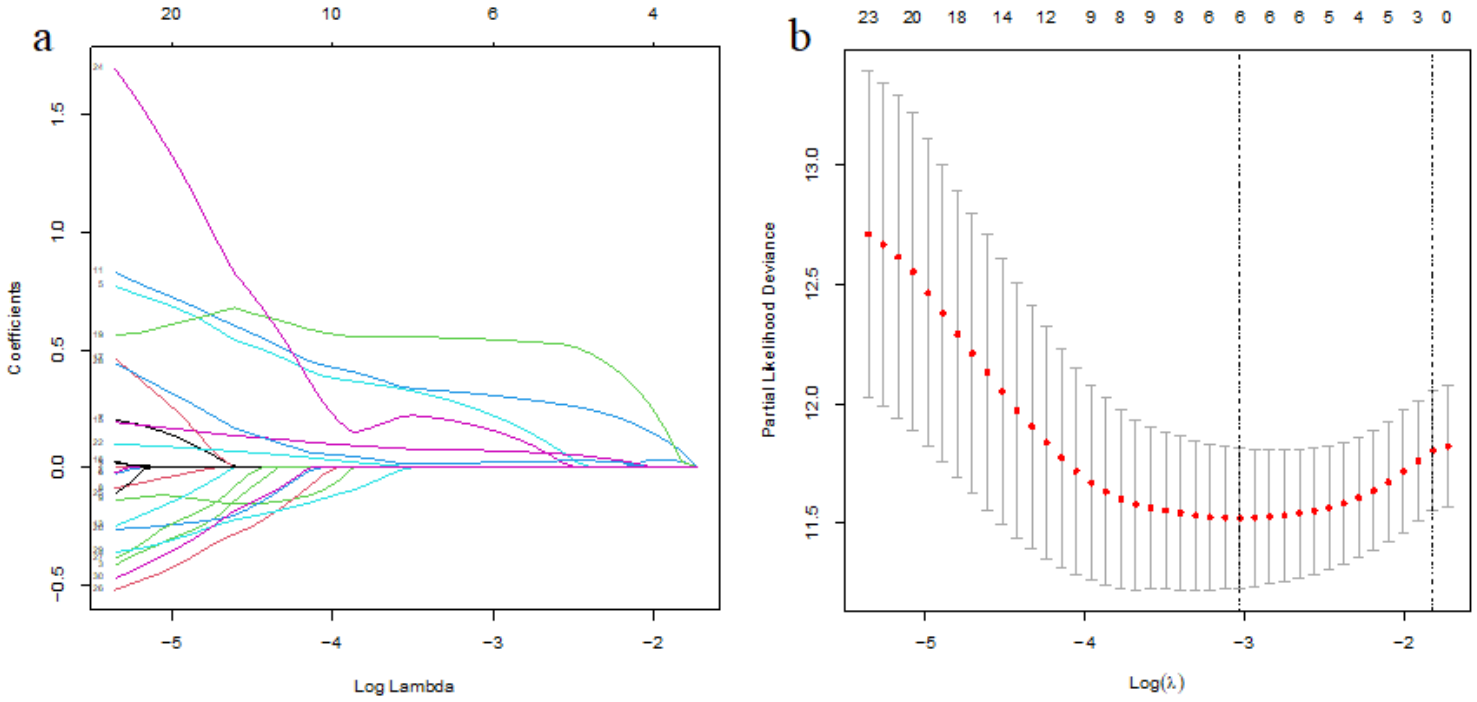

Figure 7

A risk model for ccRCC patients has been developed based on m^{6}A-related lncRNAs. (a) The perpendicular imaginary line and LASSO coefficient profile of 30 OS-related lncRNAs were drawn at the value determined by 10-fold cross-validation. (b) To cross-verify the error curve, the tuning parameters (log) of OS-related proteins were chosen. Perpendicular imaginary lines were drawn at the optimum value using the minimum criteria and 1-se criterion.

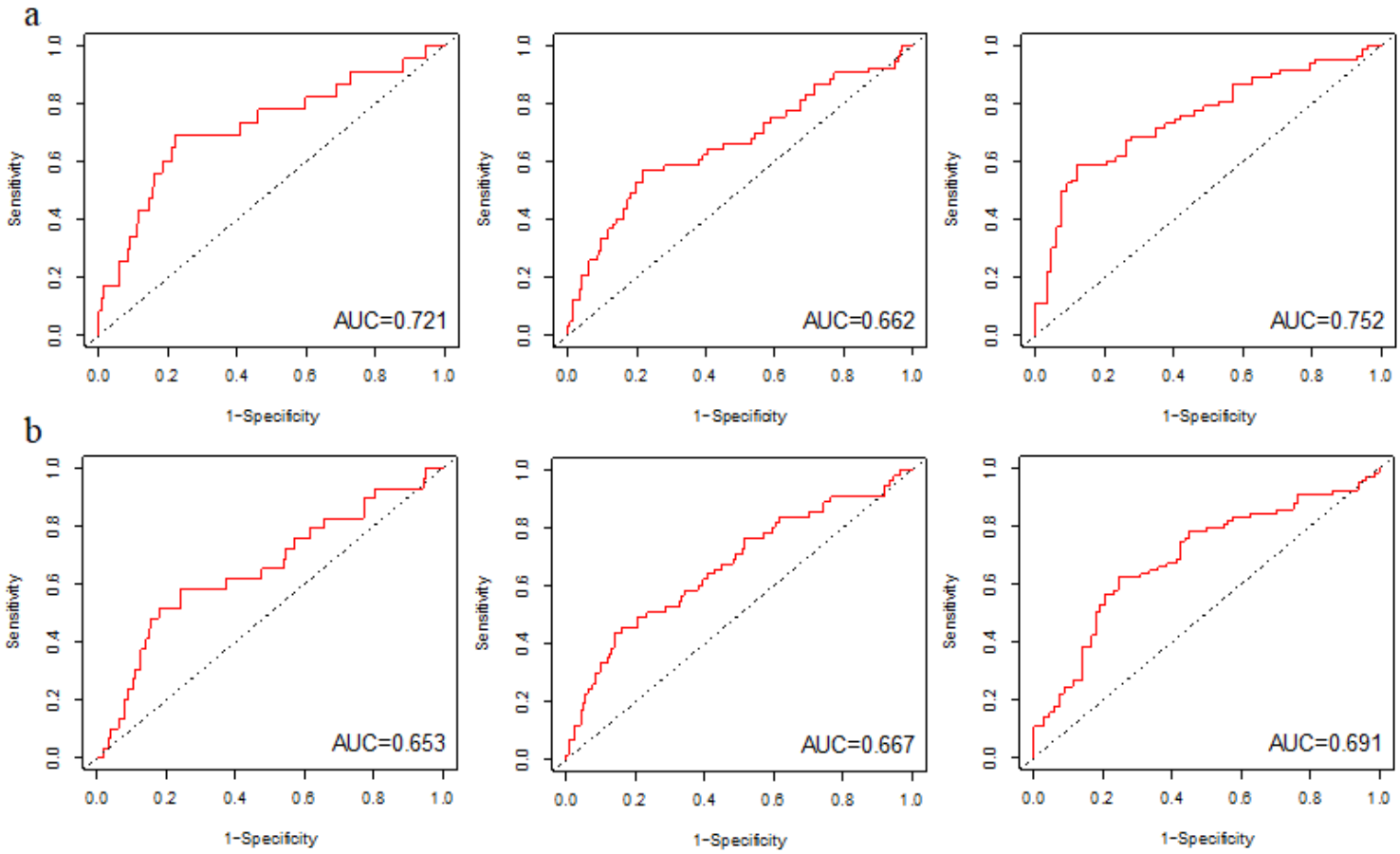

Figure 8

ROC curves evaluating the predictive value of the risk score in the high-risk group (a) and the low-risk group (b) in relation to overall survival.

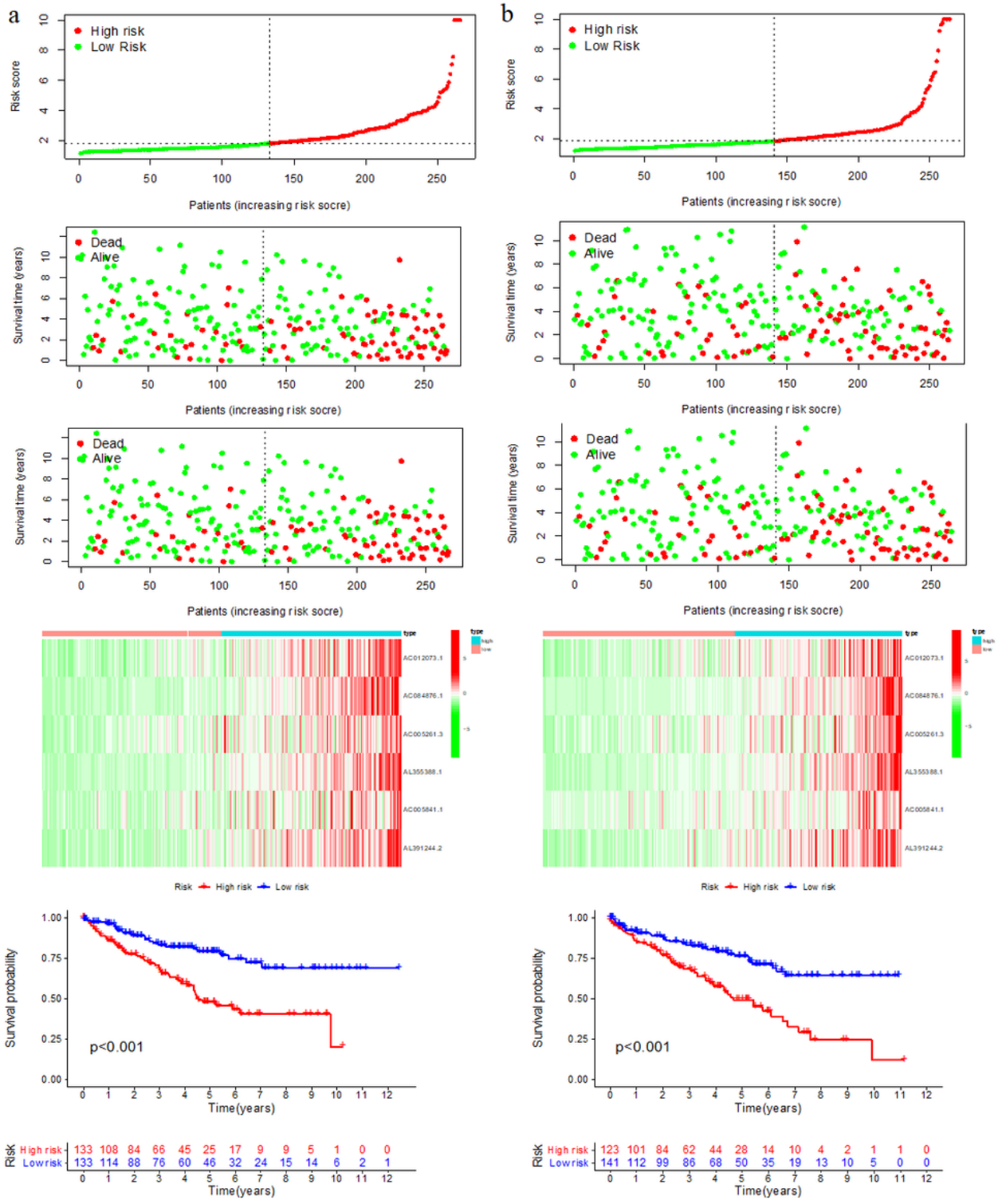

Figure 9

Construction and validation of m^{6}A-related lncRNA prognostic signatures. In the training and test cohorts, there was a distribution of risk score, OS, and OS status, as well as a heatmap of the 6 prognostic m^{6}A-related lncRNA signatures. The training cohort (a) and testing cohort (b) Kaplan-Meier curves of OS for patients with ccRCC depending on the risk score (b).

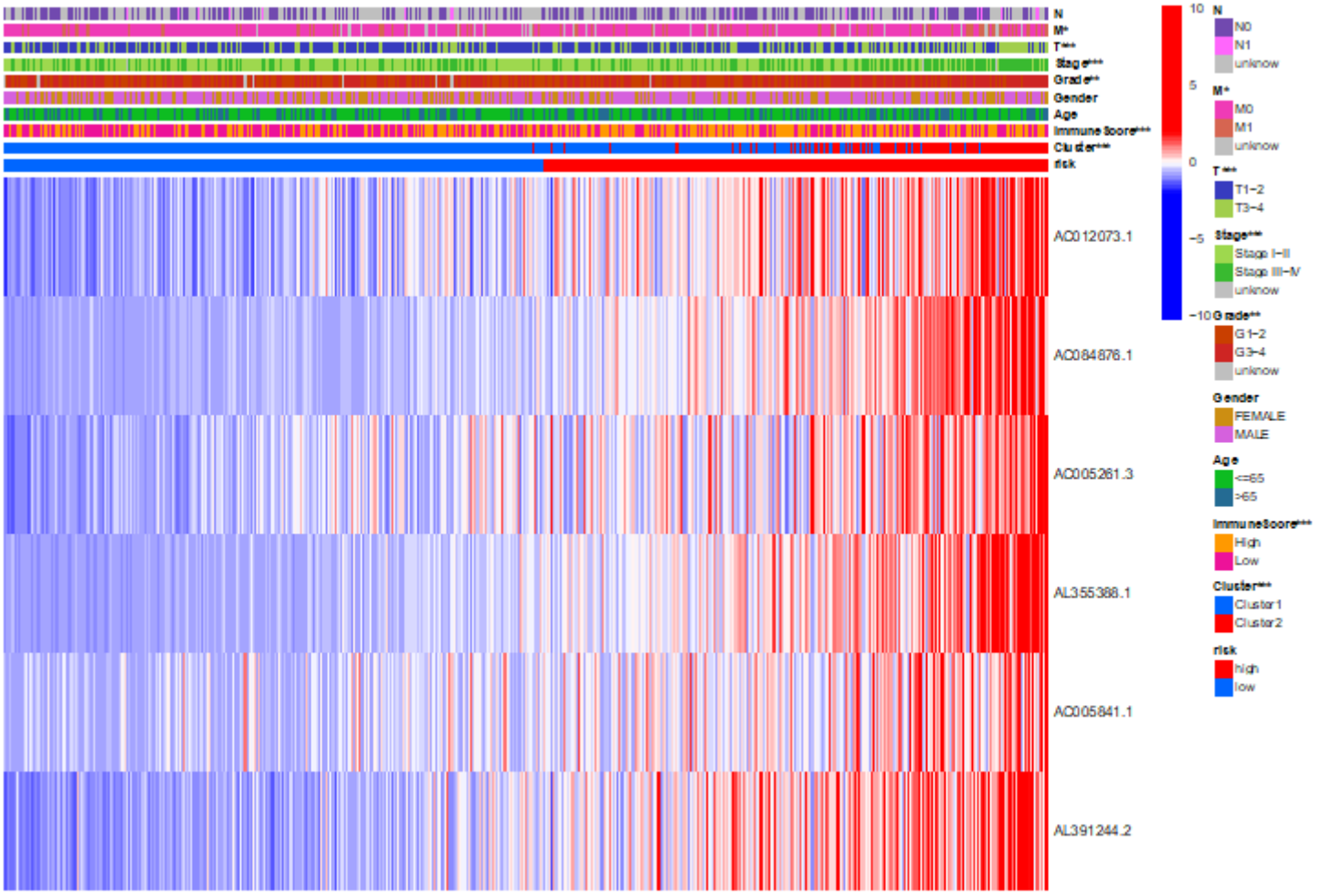

Figure 10

Heatmap illustrating expressions of m^{6}A-related lncRNAs and clinicopathologic characteristics in high- and low-risk groups.

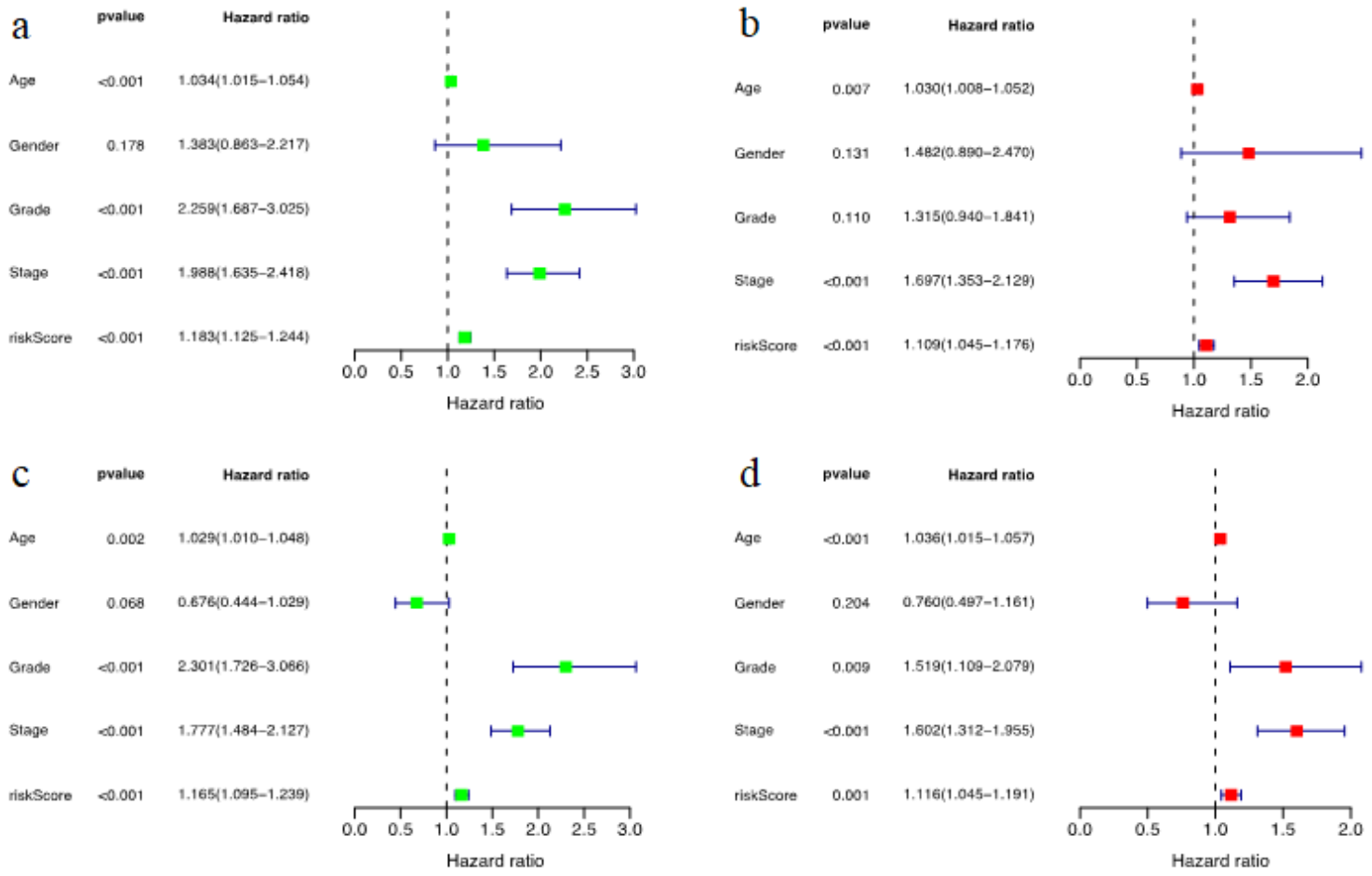

Figure 11

Prognostic analysis using both univariate and multivariate methods. Uni-(a) and multi- (b) independent prognostic analysis for training cohort. Uni- (c) and multi- (d) independent prognostic analysis for test cohort.

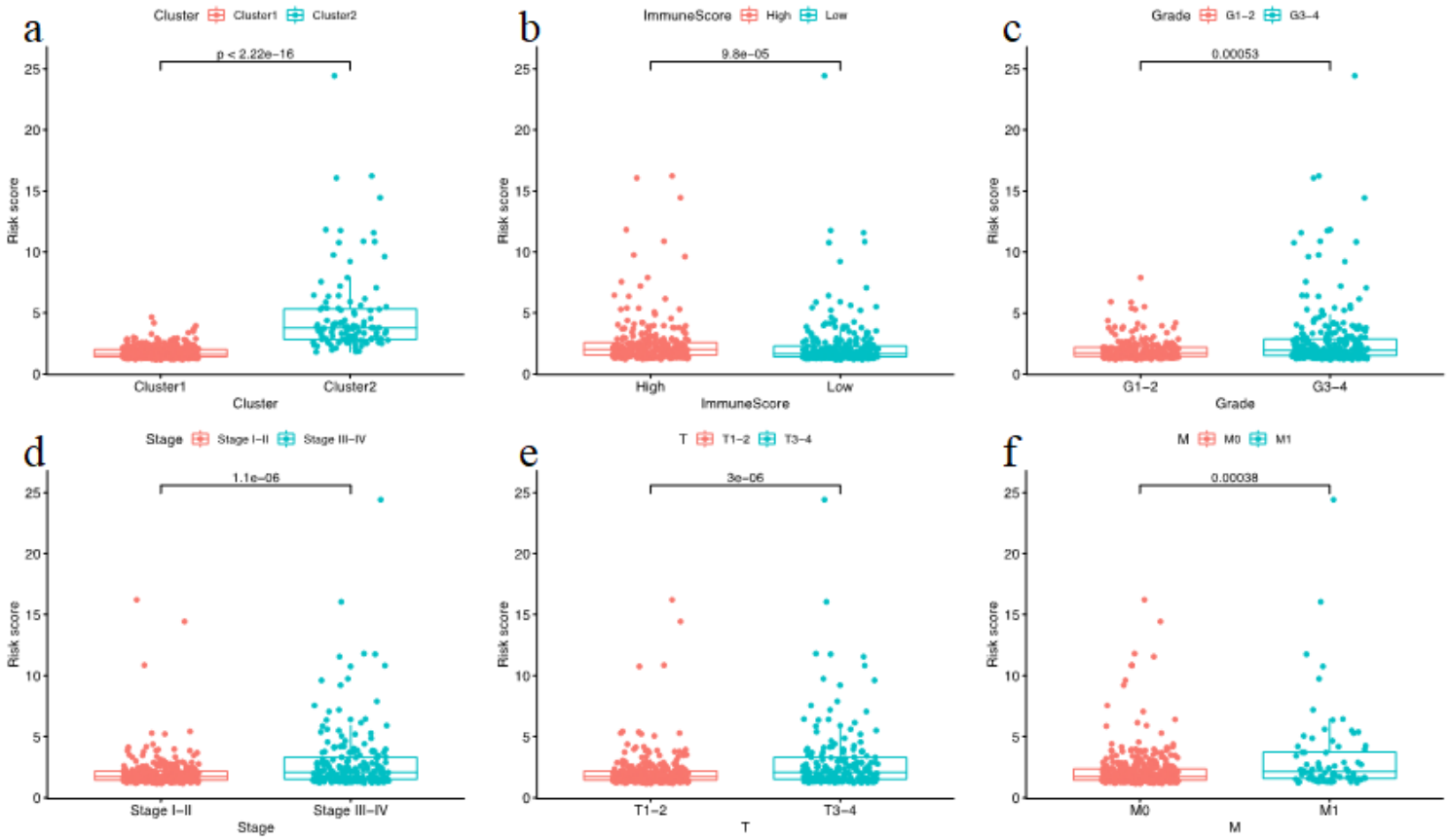

Figure 12

Distribution of risk scores stratified by cluster1/2 (a), immune score (b), grade (c), Stage (d), T stage (e) and M stage (f).

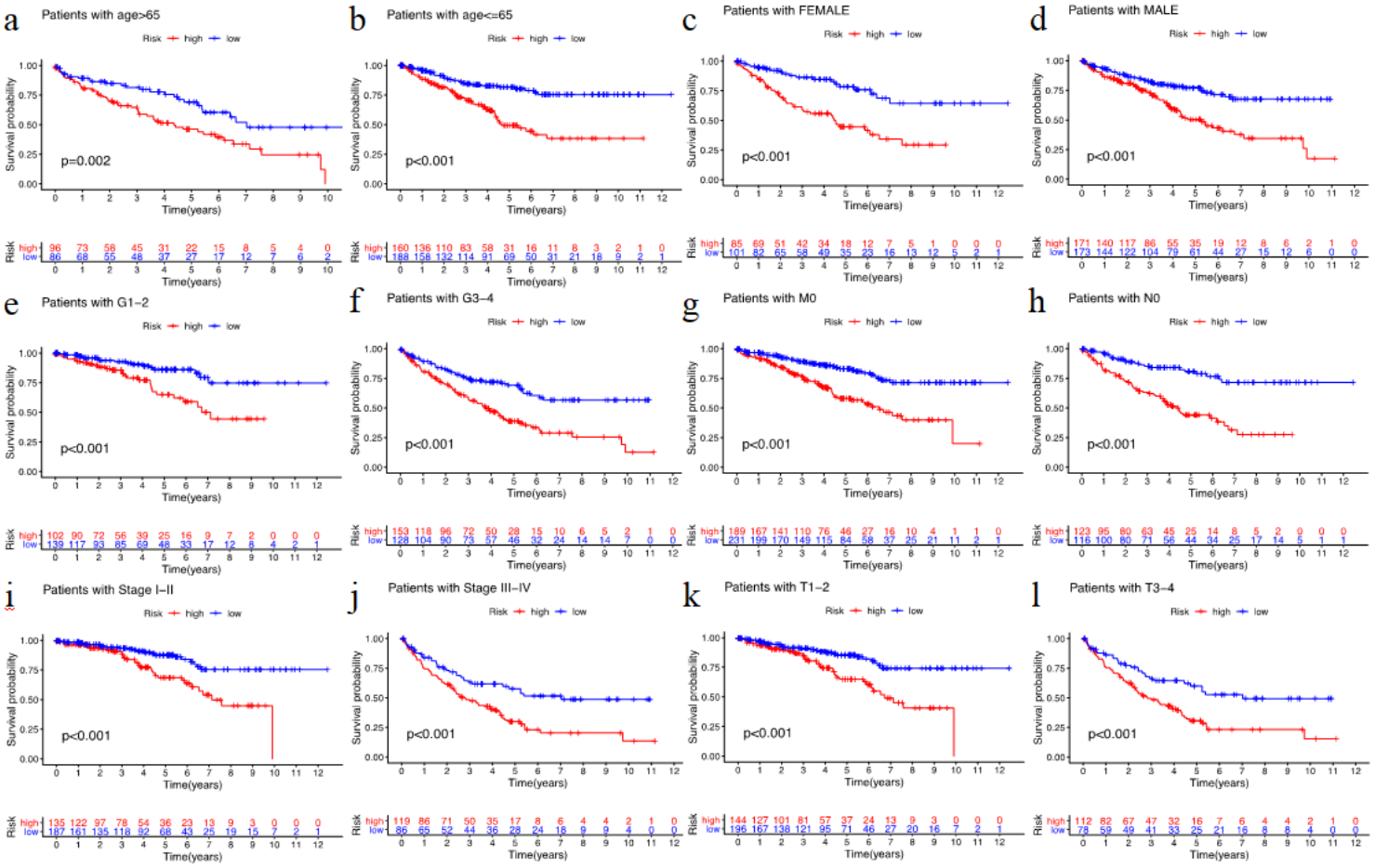

Figure 13

Model validation of clinical grouping clinical grouping (high- and low-risk group) in our study was suitable for□65 years old (a), ≤65 years old (b), female (c), male (d), G1-2 (e), G3-4 (f), M0 (g), N0 (h), stage I-II (i), stage III-IV (j), T1-2 (k) and T3-4 (l) patients.

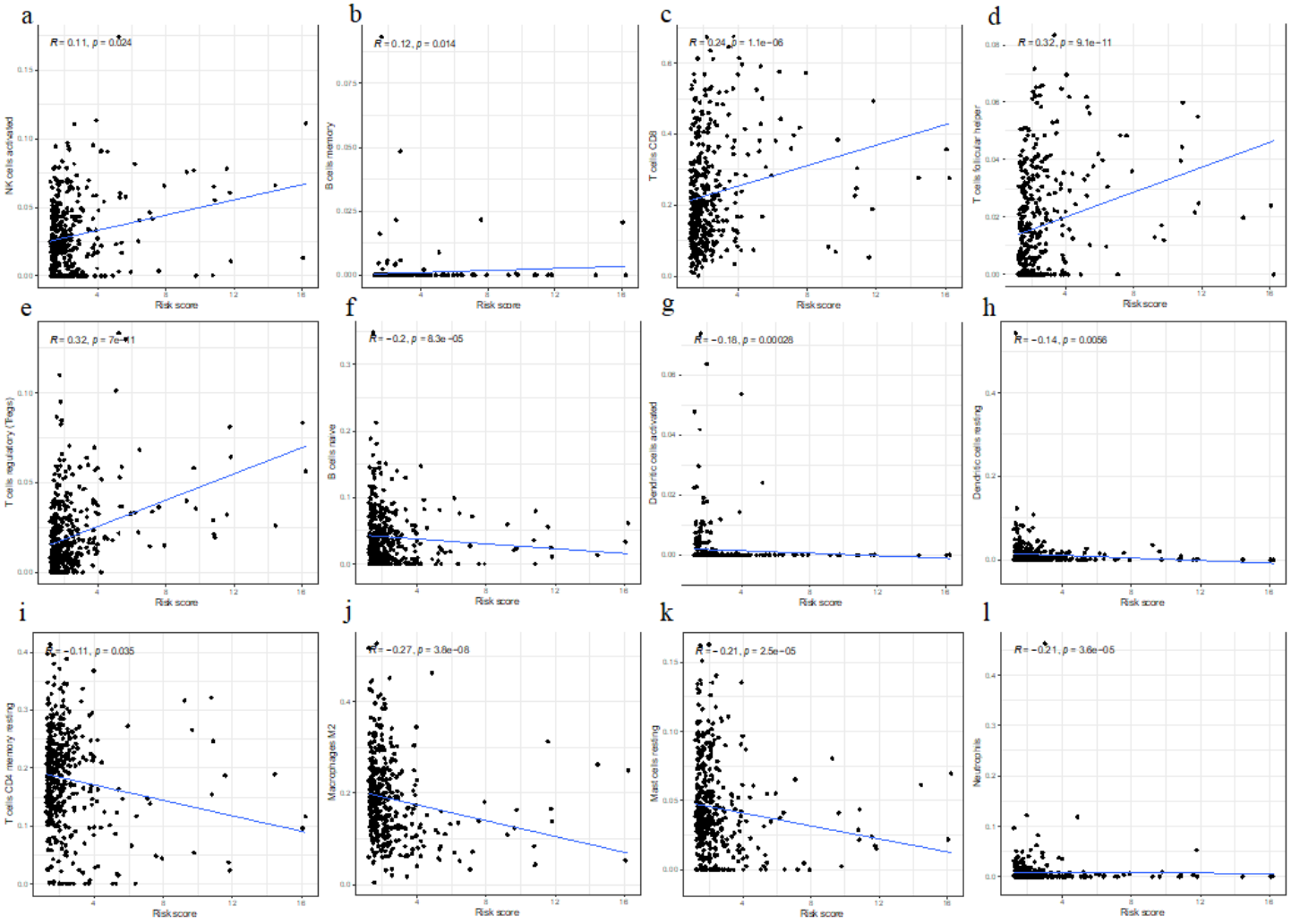

Figure 14

Analysis of the correlation between patients' risk score and the quantity of 22 immune cell types (a–l). Activated NK cells (a), memory B cells (b), $CD8^+$ T cells (c), follicular helper T cells (d), Tregs (e), naive B cells (f), activated dendritic cells (g), resting dendritic cells (h), resting memory $CD4^+$ T cells (i), M2 macrophages (j), resting mast cells (k), neutrophils (l).